Modeling the energetic tail of a dusty plasma's electron energy distribution and its effect on dust grain charge and behavior

André Nicolov[1] and Paul M. Bellan[1]
Applied Physics and Materials Science. Caltech. Pasadena. CA 91125. USA

(*Electronic mail: anicolov@caltech.edu)

(Dated: 25 June 2024)

A model for a weakly-ionized dusty plasma is proposed in which UV or X-ray radiation continuously creates free electrons at high energy, which then cool through collisions with a cold neutral gas before recombining. The transition of a free electron from high energy at birth to low energy at demise implies that the electron energy distribution is not the simple Maxwellian of an isolated system in thermal equilibrium, but instead has a high-energy tail that depends on the recombination time. This tail can have a major effect on dust grain charging because the flux of tail electrons can be substantial even if the density of tail electrons is small. Detailed analytic and numerical calculations of dust grain charging show that situations exist in which a small high-energy tail dominates charge behavior. This implies that dust grain charge in terrestrial and space dusty plasmas may be significantly underestimated if a Maxwellian distribution is assumed and the non-thermal dynamics are neglected.

I. INTRODUCTION

In many planetary and cosmic environments, microscopic grains of dust or ice exist in the presence of a weakly-ionized background gas. Examples include comet tails,[1] Saturn's rings,[2] interstellar dust clouds,[3,4] noctilucent clouds in the Earth's mesosphere,[5,6] and aerosols in the atmospheres of Titan and Pluto.[7,8] In astrophysical and atmospheric plasmas, ionization of a background gas is typically caused by stellar radiation, X-rays, or cosmic rays. Electrons and ions from the background plasma impact the dust grains and stick, causing them to accumulate large amounts of charge. Resulting electromagnetic interactions between the plasma and the dust grains cause dynamics distinct from both a dust-free plasma and a plasma-free dust cloud.

Dust charging can lead to significant macroscopic effects. For example, the dust particles of Saturn's B ring can form radial spokes through electrostatic forces, which only appear when Saturn's orientation relative to the Sun creates the proper conditions for dust to accumulate large amounts of charge.[2] Comets experience a large range of plasma conditions due to their elliptical orbits and the variability of the solar wind, which have large effects on the behavior of the coma and tail.[9] Plasma conditions can also affect the nucleation and growth of dust particles from background molecules: Ivlev *et al.*[4] showed that the charge developed on dust grains in molecular clouds greatly affect dust coagulation, Chai and Bellan[10] showed that the spontaneous formation and growth of ice grains inside a low-temperature plasma was heavily dependent on plasma properties, a process also thought to occur under astrophysical conditions. Noctilucent cloud formation in the polar mesosphere also depends on ambient temperature, and is correlated with an increase of ionization in the ionosphere's E-layer.[11] These examples indicate that the in-situ formation and behavior of dust grains is inextricably linked to the ambient plasma properties. As instruments such as JWST and ALMA become capable of imaging distant astrophysical dust clouds and low-temperature plasmas, careful treatment of dust-plasma charge interactions is important for interpreting a growing body of data.

Dust grain charging depends on the distribution of electron and ion energies present in the plasma. Traditional analysis of charging process begins by assuming that both electrons and ions are in thermal equilibrium at some defined temperature.[12] This is common in studies of atmospheric and space phenomena, including studies of noctilucent clouds[5,13] and comets.[9] This implicitly applies a Maxwellian distribution, and is often justified by invoking the high collisionality of these plasmas.[12,14,15] However, dusty plasmas generally maintain their state of weak ionization via energy input from some external ionization source; consequently, these plasmas cannot be considered isolated systems, and so may not come to thermal equilibrium. Instead, even very collisional plasmas can have a high-energy tail of hot, newly-ionized free electrons that have not yet undergone sufficient collisions to cool to the neutral temperature. As such, direct measurements of electron energies in many dusty plasmas do not show a thermal distribution: laboratory RF dusty plasmas experience stochastic heating and plasma sheath effects that accelerate a proportion of electrons,[16,17] and electron energies in the magnetosphere and other heliosphere environments are more successfully modeled by fitting functions such as the kappa distribution.[18]

Even small deviations of electron energies from a Maxwellian distribution can have disproportionately large effects on the charge and dynamics of dust grains. In a study of dust clouds embedded in plasma, Havnes *et al.*[14] showed that the relationship between cloud density and dust grain potential in plasmas with two different electron distributions yielded qualitatively similar, but quantitatively very different results. Stangeby[19] showed that a small nonthermal population of hot electrons in a Tokamak edge plasma dominated the current flux to bodies immersed in the plasma. Chen[16] identified similar behavior in RF plasmas used for manufacturing, where small numbers of hot electrons dominated the charging of Langmuir probes. These studies show that the dust charge and dynamics are extremely sensitive to slight changes in the population of high-energy electrons, so great care must be taken in handling the energy distributions for accurate cal-

culation dust characteristics.

Non-thermal electrons can greatly affect charge and dynamics in dusty plasmas, but calculations typically neglect these effects in the absence of direct electron energy measurements. We introduce a model for an enhanced energetic electron tail in a weakly-ionized plasma based on the fundamental collisions between electrons, ions, and neutrals, and characterize how this tail affects the charging of dust grains immersed in such a plasma.

II. MODEL OF THE ENERGETIC ELECTRON TAIL IN A DUSTY PLASMA

Dusty plasmas are commonly weakly-ionized, with neutral gas that is typically cold, e.g., at 10-150 K in astrophysical, planetary, and mesospheric plasmas, and near room-temperature for most laboratory dusty plasmas.[20] A tiny fraction of the gas is continuously ionized, often by UV or X-ray radiation, creating free electrons at energies of the order of a few eV. As neutrals greatly outnumber charged particles, the energetic electrons lose their initial energies through collisions with the cold neutral population, until eventually undergoing recombination. This sequence is outlined in Fig. 1.

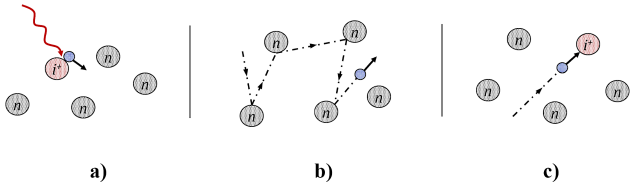

FIG. 1. a) a neutral atom is ionized by some source (red arrow), accelerating an electron (blue); b) The electron collides with many neutral atoms which "moderate" its energy; c) the electron collides with an ion and recombines.

This process is analogous to the energy moderation of neutrons used in nuclear fission reactors: in these devices, fast neutrons collide with heavier molecules, such as water or graphite, which "moderate" the kinetic energy of the neutrons and bring them towards a colder thermal distribution before entering a reactor.[21] Similarly, newly-ionized electrons can be modeled undergoing energy "moderation" through collisions with cold neutrals before recombination. At any given moment, the plasma contains both "new" electrons at high energy and a range of other electrons at intermediate stages of the moderation process. The energy distribution then depends on the processes and rates of ionization, recombination, and electron-neutral collisions.

A. Time-evolution of the energy of a single electron

The energy moderation of a hot electron in a cold neutral gas is treated for the case of elastic collisions, in the absence of external fields or turbulence. This is simplified by assuming that neutral atoms are at a constant energy kT_n, and that neutral mass $M >> m_e$. The change in electron kinetic energy in a single collision is therefore estimated by:

$$\Delta w = -\frac{4M/m_e}{(1+M/m_e)^2}(w-kT_n) \approx -4\frac{m_e}{M}(w-kT_n). \quad (1)$$

The number of collisions in a time interval dt is dt/t_{en} where t_{en} is the electron-neutral collision time. The change of electron energy dw in the time interval dt is therefore:

$$dw \approx -4(w-kT_n)\frac{m_e}{M}\frac{dt}{t_{en}} \quad (2)$$

The electron-neutral collision time is related to the mean free path of electrons, such that $v_e t_{en} = l_{mfp}$, where v_e is the electron velocity and l_{mfp} is the mean free path for electron-neutral collisions. The mean free path is related to the neutral number density n_n and the cross section for electron-neutral collisions σ_n, as follows:

$$l_{mfp} n_n \sigma_n = 1 \quad (3)$$

Using $v_e = \sqrt{2w/m_e}$, these relations can be used to substitute for t_{en} in equation 2 to obtain

$$\frac{dw}{dt} = -4\sqrt{\frac{2}{m_e}}\frac{m_e}{M}\sigma_n n_n (w^{3/2} - kT_n w^{1/2}) \quad (4)$$

Integrating from 0 to t and solving for w(t) gives,

$$w(t) = kT_n \tanh\left[2\sigma_n n_n \frac{\sqrt{2m_e kT_n}}{M} t + \tanh^{-1}\sqrt{\frac{w(0)}{kT_n}}\right]^2 \quad (5)$$

Equation 5 is plotted in Fig. 2. At t = 0, the electron is at its initial energy, $w(0)$, and energy decreases with time due to collisions.

This elastic model is appropriate for an atomic gas such as helium; for molecular gasses, the cooling rate is enhanced by rotational and vibrational effects, so this calculation should be modified somewhat. The energy drop per elastic collision, $4m_e/M$ is generalized to an overall cooling coefficient, which is in general dependent on temperature. Huxley[22] calculates the energy drop per collision with molecular hydrogen and finds the cooling to be enhanced by a factor of 2 to 4 depending on electron energy. Smith and Dean[23] experimentally measured the temperature drop of a population of electrons in an afterglow plasma undergoing collisions with N_2 and O_2 gasses, and found similarly that the cooling was 2 to 3 times faster than expected from elastic collisions alone. These studies measured the temperature drop of a bulk of electrons rather than the energy drop of a single electrons, but as both cool through electron-neutral collisions, the modification of cooling rate due to inelasticity will be of the same magnitude. The effect of inelastic collisions on the cooling curve (Eqn. 5) is equivalent to the effect of decreasing the neutral mass by a factor of 2-3, as this modifies Δw (Eqn. 1) by the same amount. Fig. 2a) shows that this causes a faster energy loss: for example, elastic collisions with molecular nitrogen follow the $M = 28m_p$ curve, while those from inelastic collisions, with energy losses 2 to 3 times larger per collision, would better fit the $M = 14m_p$ curve.

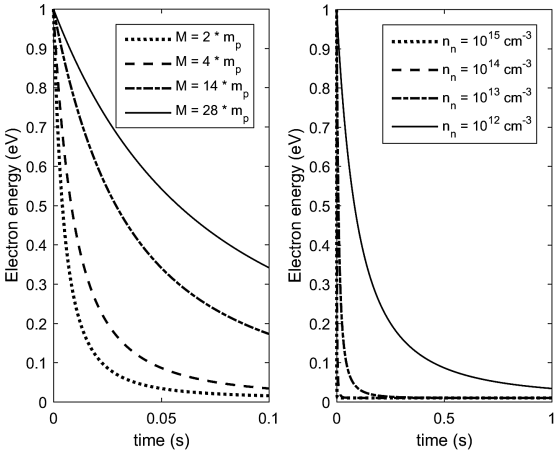

FIG. 2. Time-evolution of the kinetic energy of a single electron. a) neutral atomic mass varying from 2 to 28 m_{proton}; neutral density fixed at 10^{13} cm^{-3}. b) neutral density varying from $10^{12} - 10^{15}$ cm^{-3}; atomic mass of 4 m_{proton}. In all cases, initial energy $w(0)$ = 1 eV; target neutral particles have cross-sectional radius of 1 Å.

B. Treatment of ionization and recombination

The electron density and energy distribution depend on the ionization and recombination properties. In space and atmospheric environments, ionization is typically by high-energy photons or cosmic rays incident on both neutral gas and dust grains. The electron production rate is given by:

$$Q_e = (n_n \sigma_n + n_d \sigma_d Y)\Phi_p \tag{6}$$

where Φ_p is the incoming photon flux (m^{-2} s^{-1}), Q_e is the electron production rate (electrons/m^3/s), $n_{n,d}$ and $\sigma_{n,d}$ are the densities and photoionization cross-sections of neutrals and dust grains, respectively, and Y is the photoelectric yield of dust grains. Typically, dust densities are much lower than neutral densities,[2,17,24] and photoelectric yields are on the order of 10^{-2} or lower,[25] so neutral ionization forms the bulk of electron production.

The initial electron energy after gas photoionization depends on the difference in energy between the ionizing radiation and the ionization energy of the neutral species. All free electrons ionized from a given gas species by a specific photon wavelength then have the same initial energy.[26] While in principle there is a broad spectrum of incoming ionizing radiation, and several neutral species in the gas, there are typically certain wavelengths that dominate electron production in any given situation. For example, solar system dusty plasmas are mainly ionized by a few dominant H and He lines in the solar spectrum in the EUV range. Reid[24] shows that in the lower ionosphere, electron production is almost solely from ionization of nitric oxide by solar Lyman-α, which produce electrons at 1.1 eV. While ionization of other molecules by other parts of the solar spectrum do occur, their contribution is orders of magnitude smaller. The upper ionosphere and other solar system plasmas are mainly ionized by solar x-rays and extreme UV radiation.[24,27] As these EUV solar lines generally decrease in strength for higher photon energy,[28] most neutrals are ionized with the lowest-energy line capable of doing so. This causes electrons to have a fairly uniform initial energy in the range of 1-2 eV.

If electron and ion densities are in steady-state, ionization and recombination occur at equal rates. Recombination can occur by two mechanisms: electrons can intercept ions and recombine, or electrons and ions can intercept dust particles, stick to them, and eventually recombine on the dust particle's surface. This is modeled by the system,

$$\begin{aligned} \frac{dn_e}{dt} &= Q_e - \alpha n_e n_i - D_e n_e n_d = 0 \\ \frac{dn_i}{dt} &= Q_i - \alpha n_e n_i - D_i n_i n_d = 0 \end{aligned} \tag{7}$$

where α is the ion-electron recombination coefficient, $D_{e,i}$ is the coefficient of collection on the dust of electrons or ions. When photoemission from dust is negligible, $Q_e = Q_i$. As dust has a constant charge in equilibrium, the inflow of electrons and ions to its surface are equal: therefore, $D_e n_e = D_i n_i$. The electron density is then given by:

$$n_e = \frac{Q_e}{\alpha n_i + D_e n_d} \equiv Q_e \tau_R. \tag{8}$$

Therefore, the electron density is proportional to the average lifetime of electrons in the plasma. The lifetime can be expressed in two parts, one for electron-ion recombination and one for electron-dust collection, which add in parallel. The recombination coefficient α depends on the cross-section of collisions multiplied by the incoming electron velocity. This cross-section typically increases as energy decreases in this energy range,[29] such that recombination becomes more likely as electron energy is moderated. Meanwhile, as negatively-charged dust grains repel incoming electrons, the highest-energy electrons are more likely to be absorbed by dust grains. The lifetime of electrons in the plasma is thus dependent on the electron distribution.

C. Solution for electron energy distribution

The energy evolution of an average electron is now completely defined by equations 5 and 7, for given densities, initial energy $w(0)$, and recombination time τ_R. The fraction of the whole electron population with energy between w and $w+dw$ is defined as $f(w)dw$, and is proportional to the time spent by a single electron in that range.

This electron energy distribution must also be multiplied by the probability $p(w)$ that an electron has *not* recombined before reaching an energy w. In general, the average electron will recombine after some lifetime τ_R, with a spread of lifetimes between different electrons given by $p(w)$. Thus, the electron energy distribution is given by:

$$f(w) = A p(w) / \left| \frac{dw}{dt} \right|. \tag{9}$$

where $p(w)$ is the probability that an electron reaches an energy w without recombining, and A is a normalization factor.

The probability that a single electron recombines in some time step dt depends on the recombination cross-section, the electron velocity, and the density of ions it can recombine with. As detailed in the appendix, it follows the differential equation:

$$\frac{dp}{dt} = -n_i\sqrt{\frac{2}{m_e}}\sigma_R(w)w^{1/2}p. \tag{10}$$

The functional form of p depends on the energy dependence of the recombination cross-section $\sigma_R(w)$. Assuming a dependence $\sigma_R(w) = \gamma/w$, where γ is a constant, and putting in terms of energy rather than time by applying Eq. 4, this is evaluated to be:

$$p(w) = \left(\frac{w(0)-kT_n}{w(0)}\frac{w}{w-kT_n}\right)^{-c/kT_n} \tag{11}$$

where $c = \gamma M n_i/4\sigma_n m_e n_n$. Derivations of equations 10 and 11 are shown in the appendix.

The shape of Eq. 11 shows that probability of an electron *not* recombining is 1 for energies $w >> c/kT_n$, and drops to zero at lower energies due to high likelihood of recombination. When $c/kT << 1$, the drop in probability happens very rapidly, indicating that the spread electron lifetimes is small. Because c depends on the ionization fraction n_i/n_n, and the plasmas addressed in this study are typically very weakly ionized ($n_i/n_n < 10^{-10}$), the probability is unity until dropping to zero rapidly at a low energy. The spread in electron lifetimes is therefore small in these plasmas, and $p(w)$ can be approximated as 1 for energies between $w(\tau_R)$ and $w(0)$, and zero at energies below $w(\tau_R)$.

The normalization factor A must now be calculated, such that the integral of the distribution over all energies evaluates to unity:

$$1 = \int_0^{w(0)} f(w)dw = \int_{kT_n}^{w(0)} A\frac{p(w)}{|dw/dt|}dw. \tag{12}$$

Integrating $p(w)$ is generally quite difficult analytically; however, when all electrons are taken to recombine at the average recombination energy $w(t_R)$ as discussed, the normalization is greatly simplified:

$$A = \frac{1}{\int_{w(\tau_R)}^{w(0)}\frac{dw}{|dw/dt|}} = -\frac{1}{\int_0^{\tau_R}\frac{1}{|dw/dt|}\frac{dw}{dt}dt} = \frac{1}{\int_0^{\tau_R}dt} \tag{13}$$

Therefore, $A = 1/\tau_R$, and the electron energy distribution is expressed as follows:

$$f(w) = \frac{M}{4\tau_R\sqrt{2m_e}\sigma_n n_n}\frac{1}{w^{3/2}-kT_n w^{1/2}}. \tag{14}$$

$f(w)$ is plotted in Figure 3 for lifetimes of 0.05, 0.1, and 1 seconds at a plasma parameters common to planetary and astrophysical environments. This is compared to a Maxwellian distribution at a temperature of 0.01 eV, expected if electrons were in thermal equilibrium with the neutrals. It is clear that the high-energy tail of the distribution is much larger than the Maxwellian tail. As recombination time increases, more electrons will reach low energies; however, the high-energy tail remains larger than Maxwellian. Figure 4 shows the distribution for recombination times from 10 seconds to an hour on a logarithmic scale, so that the deviation between the Maxwellian and calculated distribution is more evident. The Maxwellian tail trends towards zero at an exponentially faster rate, showing the moderation model will always have a larger hot tail than the Maxwellian distribution predicts.

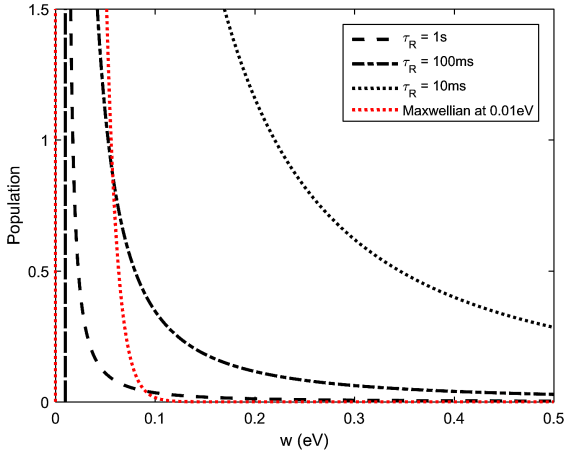

FIG. 3. Electron energy distributions for various recombination times. Low-temperature Maxwellian (red dotted line) is at 0.01 eV. Target neutral particles have cross-sectional radius of 1 Å; neutral density is 10^{14} cm^{-3}, neutral atoms have mass $M = 4 * m_{proton}$, and initial electron energy $w(0)$ is 1 eV.

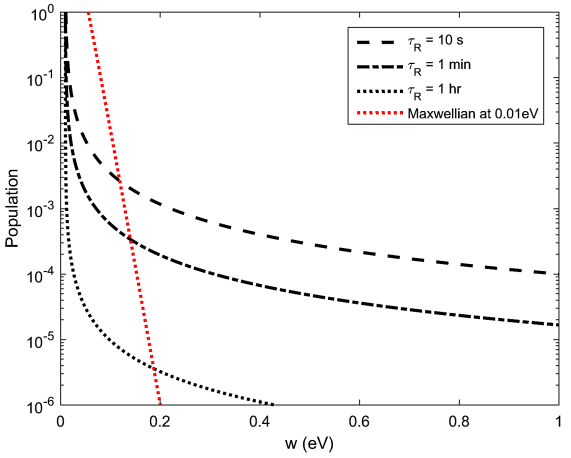

FIG. 4. Electron distributions for recombination times ranging from 10 sec to 1 hr, plotted on a log scale. Initial energy $w(0) = 1$ eV, target neutral particles have cross-sectional radius of 1 Å, neutral density is 10^{14} cm^{-3}, and neutral atoms have mass $M = 4 * m_{proton}$. Maxwellian (dotted line) at 0.01 eV.

III. QUANTIFYING THE CHARGING PROCESS

Dust grains generally gain charge through two mechanisms: the collision and sticking of electrons and ions in the plasma, and photoemission from incident high-energy radiation. The former causes the dust charge to be negative, and the latter positive. A dust grain attains charge equilibrium when all charging mechanisms balance, resulting in a zero net current to the dust grain surface. Plasma micro-instabilities and variable radiation conditions can sometimes cause further dynamic changes in dust charge;[17] these effects are beyond the scope of this paper.

When neutral gas density is significantly higher than dust grain density, collisions with charged particles typically dominate over photoemission. For example, under conditions of noctilucent clouds formation, we calculate that the incoming electron flux to a water-ice grain 10 nm in radius[6] is an order of magnitude larger than the outgoing electron flux from photoemission.[25] This is supported by observations of negative charge on these mesospheric dust grains.[5] Similarly-large negative charges are also seen in Saturn's rings.[2] Furthermore, as photoemission is dependent only on the grain's photoelectric yield, its contribution is generally constant regardless of plasma presence. Photoemission then has little effect on the changes of dust equilibrium charge with electron energies, and is neglected in the following calculations.

By charge conservation, an increase of charge comes at the expense of free electrons in the plasma. The distribution of charge between free particles and the dust grains is described by the Havnes parameter,[14]

$$H = \frac{Z_d n_d}{n_i} = 1 - \frac{n_e}{n_i} \tag{15}$$

which describes the fraction of negative charge that is attached to the dust. Here $n_{i,e,d}$ is the number density of ions, electrons, or dust grains, and Z_d is the number of charges on each dust grain. The free electron population will be depleted as the dust charge increases: as H approaches 1, the supply of free electrons is exhausted.

A. Calculation of current to an isolated dust grain

The current into the dust surface is calculated for the simple case of an isolated dust grain, for which the Debye length is much larger than the spacing between dust grains. In this case, electrons and ions only experience the electric potential from the single dust grain during the collision process. This typically holds true if the plasma density is large compared to the density of dust grains. If grains can interact, the electrostatic potential experienced by incoming electrons must be determined using Poisson's equation and treated as an N-body problem.[14]

A spherical ice grain has a geometric cross-section given by the cross-sectional area, $\sigma_{geometric} = \pi r_d^2$ where r_d is the dust grain radius. The total cross-section depends also on Coulomb attraction. Consideration of conservation of total energy and angular momentum show that the effective dust grain cross-section for a collision with a charged particles is modified[30] to be:

$$\sigma(v) = \sigma_{geometric}(1 - \frac{2q\phi_d}{mv^2}) \tag{16}$$

where q is the charge on the incoming particle, and ϕ_d is the dust grain surface potential. The cross-section is therefore larger than πr_d^2 if the charged particles are attracted to the dust grain ($q\phi_d < 0$) and smaller if the charged particles are repelled ($q\phi_d > 0$).

The current flow to the dust grain due to collisions with charged particle species is calculated for a spherical dust grain:

$$I = q\int_{v_{min}}^{\infty} \sigma(v) v f(v) 4\pi v^2 dv \tag{17}$$

where v_{min} is the minimum velocity of particles that can reach the dust grain. For a particle that is being attracted, incoming velocities within the entire range $0 \leq v < \infty$ must be considered. However, for a particle that is being repelled, particles with velocities less than $\sqrt{2q\phi_d/m}$ are reflected by the dust's electric potential and never reach the grain. By defining $f(w)dw = 4\pi v^2 f(v)dv$ and doing a change of variables, $w = \frac{1}{2}mv^2$, currents are described in terms of kinetic energy rather than velocity:

$$I_{attractive} = q\sqrt{\frac{2}{m}}\int_0^{\infty} \sigma_R(w)\sqrt{w} f(w) dw \tag{18}$$

$$I_{repulsive} = q\sqrt{\frac{2}{m}}\int_{q\phi_d}^{\infty} \sigma_R(w)\sqrt{w} f(w) dw. \tag{19}$$

As the dust is generally negatively charged,[15] $\phi_d < 0$. Thus, ion current follows Eqn. 18, and electron current follows Eqn. 19. At equilibrium, a charge $Z_d e$ resides on the dust such that the ion and electron currents are equal.

The current balance therefore depends on the energy distributions $f_i(w)$ and $f_e(w)$. Equation 16 indicates that, for a negatively-charged dust particle, the fastest electrons have the largest cross-section, meaning the high-energy tail of the distribution is most important. Conversely, the slowest positive ions have the largest cross section; therefore, a Maxwellian distribution at neutral gas temperature is sufficient for calculating ion current to the dust. Consider a Maxwellian ion distribution:

$$f_i(w) = 2n_i\sqrt{\frac{w}{\pi(kT_i)^3}}\exp(-\frac{w}{kT_i}). \tag{20}$$

By substituting this into equation 18 and simplifying, the ion current is evaluated to be

$$I_i = \pi r_d^2 \frac{2en_i}{\sqrt{\pi}}\sqrt{\frac{2kT_i}{M}}(1 - \frac{e\phi_d}{kT_i}). \tag{21}$$

Here it is assumed $q_i = e$, as ions in dusty plasmas are typically singly-ionized. As dust charging is more sensitive to the

electron distribution, the electron current is written in terms of an arbitrary distribution,

$$f_e(w) = n_e g(w). \tag{22}$$

The electron current is then calculated from Equation 19:

$$I_e = e n_e \pi r_d^2 \int_{-e\phi_d}^{\infty} \sqrt{\frac{2}{m_e}} (1 + \frac{e\phi_d}{w}) \sqrt{w} g(w) dw. \tag{23}$$

It is useful to write the dust potential ϕ_d in terms of a dimensionless variable; we normalize it by dividing by the ion thermal energy,

$$\psi_d = -e\phi_d / kT_i. \tag{24}$$

The current balance between electron and ion flows is rewritten for Maxwellian ions and an arbitrary electron distribution.

$$\frac{2n_i}{\sqrt{\pi}} \sqrt{\frac{kT_i}{M}} (1 + \psi_d) = \frac{n_e}{\sqrt{m_e}} \int_{kT_i\psi_d}^{\infty} (1 - \psi_d \frac{kT_i}{w}) \sqrt{w} g(w) dw. \tag{25}$$

B. Calculating plasma equilibrium with charged dust

When dust charge is in equilibrium, electrons and ions collect on the dust at equal rates. Ignoring photoemission from dust grains, electrons and ions are also produced through ionization at equal rates ($Q_e = Q_i$ in Eqn. 7). The electron and ion densities will change with production and recombination until reaching steady-state values, such that $dn_e/dt = dn_i/dt = 0$.

The dust collection coefficients (D_e in Eqn. 7), is the flux of electrons to each dust grain multiplied by the dust density. Therefore, D_e and D_i can be expressed as the electron and ion currents divided by densities and charges:

$$D_e = \pi r_d^2 \int_{-e\phi_d}^{\infty} \sqrt{\frac{2}{m_e}} (1 - \psi_d \frac{kT_i}{w}) \sqrt{w} g(w) dw \tag{26}$$

$$D_i = \pi r_d^2 \frac{2}{\sqrt{\pi}} \sqrt{\frac{2kT_i}{M}} (1 + \psi_d) \tag{27}$$

Once steady state is reached, Eqn. 7 indicates that $D_e n_e = D_i n_i$. Therefore,

$$D_e = \frac{n_i}{n_e} D_i = \frac{D_i}{1 - H} \tag{28}$$

and can be formulated without information about the electron energy distribution.

As dust collection coefficients depend on the dust potential ϕ_d, more information must be known about the dust charge or the charging process to completely describe the system. This could be satisfied by solving the current balance (Eqn. 25), again requiring a known electron distribution. This could also be computed through numerical simulation, which equivalently requires assumptions about the energy of each particle. Both these methods are pursued in subsequent sections, using the previously-derived model of electron production and cooling.

IV. SIMULATING PLASMA EQUILIBRIUM WITH A MONTE CARLO METHOD

A Monte Carlo method is used to model a population of electrons, ions and dust grains of a given size, in which individual electrons are created at initial energy $w(0)$, cool over time through neutral collisions according to Eqn. 5, and eventually recombine with ions or dust grains. At each timestep in the simulation, the probability is computed for an electron colliding with an ion or a dust grain, and each electron is either chosen to recombine or remain, based on these probabilities. After a sufficient number of iterations, the simulation reaches a steady-state electron and ion densities and yields equilibrium distributions of electron energies and dust charges.

A. Methodology

The simulation methodology is as follows:

1. A control volume the size of 1 cm^3 is considered, containing an arbitrary number N_e of electrons, each at initial energy w_0. An equal number of ions is initialized, as well as N_d dust particles of radius r_d.

2. In a small timestep Δt, each electron has its energy decreased by $\Delta w(w)$, calculated from Eqn. 2.

3. For each electron, the probability of a collision with an ion, a neutral dust grain, and a dust grain of any charge, are calculated. These are dependent on electron energy.

4. A random number between 0 and 1 is generated. Depending on the value, it is chosen based on calculated probabilities whether each electron recombines with an ion, a dust grain, or remains in the plasma.

5. If the electron collides with an ion, it is removed from the simulation, and both N_e and N_i are decreased by 1.

6. If the electron collides with a dust particle of charge Z_d, the electron is removed from the simulation, and N_e is decreased. The number of dust particles with a charge Z_d is decreased by 1, and the number of grains with $Z_d + 1$ is increased.

7. The probability of ions colliding with dust grains is calculated, and a corresponding proportion of them are subtracted from N_i. The charge number of incident dust particles is decreased.

8. A number $Q * dt$ electrons at $w(0)$ and ions are added to simulate photoionization.

This process is repeated for a large number of time steps, until N_i and N_e reach equilibrium values that cause the recombination rate to balance the production rate. At this point, the electron energy and dust charge distributions are also in steady state.

B. Electron energy distributions in steady state

The steady state electron distribution depends on the competition between three rates, namely the rate of electron-neutral collisions, the rate of electron production, and the rate of electron removal. As neutral density is typically far greater than plasma or grain density, the electron-neutral collision rate is orders of magnitude larger than the rest. By defining a characteristic electron-neutral collision time $t_{en} = 1/\sigma_n n_n \sqrt{2w/m_e}$, Eqn. 5 can be rewritten in terms of the number of electron-neutral collisions $x = t/t_{en}$. This form, independent of neutral density and cross-section, is plotted in Fig. 5.

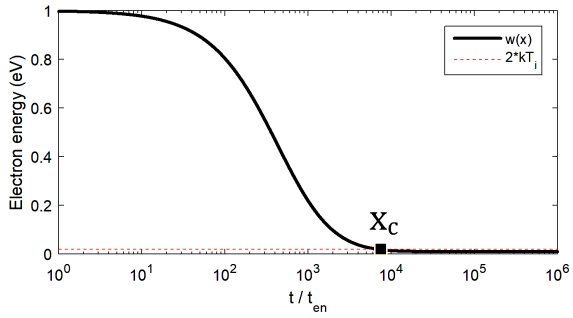

FIG. 5. Decrease of single electron energy with number of collisions. Intersection point of $w(x)$ with $2 * kT_i$ defines the critical number of collisions x_c for each electron to cool. In this plot, $w(0) = 1$eV, $kT_i = 0.01$eV, and energy transfer per collision is that of molecular nitrogen. For these values, $x_c \approx 7500$.

The electron energy decays through neutral collisions until asymptotically reaching the neutral temperature. We define a critical number of collisions x_c in which electron energy has cooled to twice the neutral temperature. This critical collision number is compared to the rates of recombination. If most electrons undergo x_c collisions before recombining ($\tau_R/t_{en} > x_c$), there will be a bulk of cold electrons in the plasma. If most electrons recombine before cooling ($\tau_R/t_{en} < x_c$), electrons will remain much hotter than the neutrals. If the electron recombination is comparable to the cooling time ($\tau_R/t_{en} \sim x_c$), the energy distribution will contain both a cold bulk and a significant high-energy tail. Resulting electron distributions for each of these cases are shown in Fig. 6.

In each of the three cases, different behavior can happen depending on if the electron production rate is large or small compared to the cooling rate. If electrons are produced more quickly than they cool, there can be a small population of hot electrons even with long recombination time. If electrons are not produced so quickly, the energetic tail will be mostly empty, and will have minimal effect on the dust.

C. Effect on dust charge distribution

When dust grains are charged to surface potentials such that $e\phi_d > w$, where w is the energy of an incoming electron, that

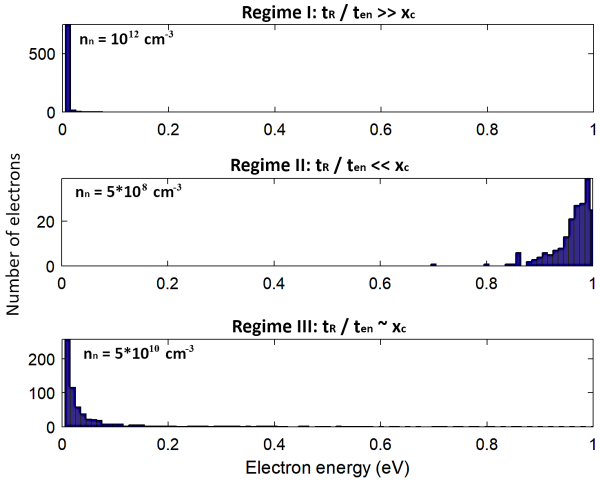

FIG. 6. Computed electron distributions for each of three regimes. All simulations had $n_d = 1000$ cm^{-3}, $r_d = 10$ nm, neutrals corresponding with molecular nitrogen. Neutral density is varied by 4 orders of magnitude to reach various regimes.

electron will be repelled. Therefore, high-energy electrons can approach grains of higher charge. Therefore, it is expected that these high-energy tails in the electron distribution allow some grains to reach larger charges than expected for a cold Maxwellian electron population.

Fig. 7 shows the number of dust grains at various charges in four different simulations. The horizontal axis corresponds to the charge number Z_d on each charged particle, and the vertical axis shows the number of dust particles with that charge. The total number of dust particles in this simulation was 1000. In Fig. 7a), all electrons were created and remained at neutral temperature for all time. Fig. 7b), c), and d), are the distributions when electrons are created at high energy and cool, each with different neutral densities; these have the same parameters as those used in cases I, II, and III in Fig. 6.

Fig. 7b) corresponds to the case when electrons cool more quickly than they recombine. In comparison to 7a), the charge distribution is very similar; this is expected, as electrons only spend a tiny fraction of their lifetimes at energies above neutral temperature. However, a fraction of dust grains in case b) are doubly-charged, while case a) only allows singly-charged grains. This shows that even though nearly all electrons are cold, high-energy tail still allows some greater amount of dust charging.

Fig. 7c) shows the charge developed when electrons don't cool much below 1 eV; here, the peak of the charge distribution is at $Z_d = 6$. As x_c is large, (e.g. 7500 in the case of Fig. 5), these plasmas are still very collisional, despite the considerable role played by a non-thermal tail of electrons. In Figure 7d), the dust grains have a distribution of charges ranging from $Z_d = 1$ to 5; this is the charge developed by electrons in the distribution shown in Fig. 6, regime III. Most electrons are still cold, but there is a larger hot tail, and this can increase the charge on dust five-fold.

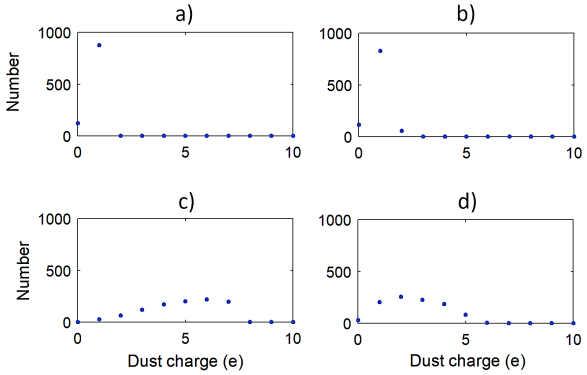

FIG. 7. Computed distributions of dust charge for each of four cases. In a), all electrons at kT_i for all time. In b), c), and d), electrons are created at 1 eV and cool through collisions with neutrals at densities $n_n = 10^{12}$, $5*10^8$, and $5*10^8$ cm^{-3}, respectively. All simulations had $N_d = 1000$, $r_d = 10$ nm, and neutrals corresponding with molecular nitrogen.

V. ANALYTIC CALCULATION OF DUST CHARGE

An analytic solution for the equilibrium state of the dusty plasma requires solution of the current balance in Eqn. 25. This is done in terms of two non-dimensional quantities: the normalized dust potential ψ_d (Eq. 24) and the Havnes parameter H (Eq. 15). By inserting these quantities into the Eq. 25 and solving for H as a function of ψ_d,

$$H(\psi_d) = 1 - \frac{\sqrt{m_e/M}(1+\psi_d)}{\frac{\sqrt{\pi}}{2}\int_{kT_i\psi_d}^{\infty}\sqrt{\frac{w}{kT_i}}(1-\psi_d\frac{kT_i}{w})g(w)dw}. \quad (29)$$

This relation characterizes the steady-state distribution of charge in the dusty plasma: H gives information about the ratio of charge carried by the dust population compared to free electrons and ions, and ψ_d describes the charge on each individual dust grain of a given size.

For a spherical grain of size r_d and charge $Z_d e$, the surface potential is:

$$\phi_d = -\frac{Z_d e}{4\pi\varepsilon_0 r_d} \quad (30)$$

so combining Eqs. 24 and 30 gives the dust charge:

$$Z_d = \frac{4\pi\varepsilon_0 r_d kT_i}{e^2}\psi_d. \quad (31)$$

Substituting H for Z_d using Eq.15 gives a linear relationship between H and ψ_d:

$$H = \frac{4\pi\varepsilon_0 kT_i}{e^2}\frac{n_d r_d}{n_i}\psi_d. \quad (32)$$

The intersection between this linear dependence of H on ψ_d and the curve calculated in Eq. 29 gives the equilibrium values of H and ψ_d for a dusty plasma with given r_d and n_d.

The electron distribution calculated in equation 14 is used for $g(w)$ in Eq. 29, which approximates the probabilistic collision process used in the Monte Carlo simulation. As this distribution applies over the energy range $w \in [w(\tau_R), w(0)]$, the upper boundary of the integral in the denominator of equation 29 is decreased from infinity to $w(0)$. The lower boundary, $w = kT_i\psi_d$, is usually larger than $w(\tau_R)$, but care must be taken when dealing with very short recombination times. Solving results in the parameter curve:

$$H(\psi_d) = 1 - \frac{\sqrt{m_e/M}(1+\psi_d)}{\sqrt{\frac{\pi}{2m_e kT_i}}\frac{M}{8\tau_R\sigma_n n_n}\left(\psi_d \ln\frac{w(0)}{kT_i\psi_d} + (1-\psi_d)\ln\frac{w(0)/kT_i - 1}{\psi_d - 1}\right)}. \quad (33)$$

This curve is plotted in figure 8, estimating ions to have the same mass and temperature as neutrals. The curve has a distinct knee-shape, in which $H = 1$ for low ψ_d, and H quickly decreases when ψ_d exceeds a critical value. When H approaches 1, no free electrons remain in the plasma. As H approaches zero, the curve implies each dust grain has a large amount of charge given by ψ_d, but nearly all electrons remain free in the plasma. It is noted from the figure that a small fraction of hot electrons significantly affects the shape of the curve: for fixed H, the curve reaches significantly higher values of ψ_d when electron lifetime is short. This shows that the distribution's greater high-energy tail dominates the charging process.

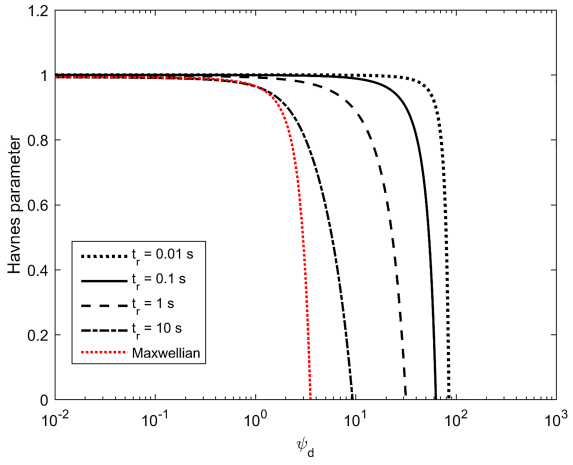

FIG. 8. Parameter curve $H(\psi_d)$ for the calculated distribution of a weakly-ionized plasma at four recombination times, for $n_n = 10^{12}$ cm^{-3}, initial energy $w(0) = 1$ eV, and atomic helium gas at 0.01 eV.

As this approach does not explicitly treat dust charge as discrete, it breaks down as Z_d approaches 1. This is typically the case when plasma density is similar to dust grain density or smaller, or when dust cross-section is very small. This approach also assumes all dust grains carry the same charge. As seen in the simulation, grains have a distribution of charges dispersed about some average value. This approximation again becomes valid when Z_d is large, as the spread

TABLE I. Comparison between results of simulation and analytical calculation, for the three cases in Fig. 6: (a) $n_n = 10^{12}$, (b) $n_n = 5*10^8$, and (c) $n_n = 5*10^{10}$ cm^{-3}. Dust has $r_d = 10$nm, n_d = 1000 cm^{-3}.

	H	ψ_d	$Z_{d,avg}$	n_e (cm^{-3})	n_i (cm^{-3})
Simulation (a)	0.46	15.40	1.07	1260	2330
Analytical (a)	0.34	14.39	1.00	1956	2956
Simulation (b)	0.96	70.04	4.86	185	5054
Analytical (b)	1.00	38.90	2.70	0.01	2703
Simulation (c)	0.73	37.49	2.61	924	3530
Analytical (c)	0.49	20.45	1.42	1470	2891

of charges is small compared to the average value. Properties calculated from the simulations shown in Fig. 6 are compared to the properties calculated analytically from the same input conditions in Table I. While these simplifications cause some divergence between the simulation and the analytical method, both show the same effect of the energetic tail on equilibrium values of ψ_d and H.

VI. APPLICABILITY TO ATMOSPHERIC AND ASTROPHYSICAL PLASMAS

The prior calculations made several simplifications. Firstly, it is assumed that electrons are mainly produced through photoionization of neutrals, rather than photoemission from dust grains. It is also estimated that electrons are produced at a fixed energy above the cold temperature of electrons and neutrals, and that electrons cool through elastic collisions with a neutral gas. In modeling the collection of plasma particles on dust grains, orbit motion-limited theory is used,[17] which requires that dust grains are sufficiently isolated and do not interact through electrostatic forces. These assumptions must hold in order to accurately apply the model to plasmas in nature; Table II lists relevant properties of terrestrial and astrophysical dusty plasmas that can be used to assess model applicability.

The assumption that photoemission is negligible has the potential to affect the charge equilibrium to the greatest extent, as photoemission can cause dust grains to charge positively, which has been observed on occasion in atmospheric[5] and comet[9] plasmas, depending on the incident radiation, local neutral density, and dust composition. As the photoemissive charging is independent of the plasma particles, it could be modeled with an extra term in the current balance (Eqn. 25) that is constant with respect to electron energy. The described effects of a hot electron tail would not differ, though they would likely be negligible compared to the high photoemissive current. Many of these plasmas contain diatomic neutral gases, which can cool electrons more rapidly than predicted by elastic collisions due to their rotational and vibrational degrees of freedom. As mentioned in Section II.A, this effect can be approximated as a constant multiple to the cooling rate $4m_e/M$ of 2 to 3, or equivalently, by dividing neutral mass by 2-3. For example, in applying the electron moderation model to plasmas with N_2 gas, an effective mass of $N = 28m_p/3$ is used. It was also previously discussed that solar system plasmas can usually be approximated as producing electrons at constant energy, as the solar spectrum has discrete peaks in the ionizing range; this does not hold for molecular clouds, which are mainly ionized by cosmic rays, as cosmic rays have a much broader spread of incident energies.[4]

Different plasmas cool to different extents: for example, noctilucent clouds, comet tails, and protoplanetary disks are typically assumed to have electrons and neutrals at similar cold temperatures due to their collisionality. The electrons in Saturn's rings, however, have been shown to be hotter;[2] This is explained by the fact that neutral density is low, so electrons will not cool before recombining. Therefore, protoplanetary disks are in the $\tau_R/t_{en} > x_c$ regime, while Saturn's rings have $\tau_R/t_{en} << x_c$. As shown previously by the simulations in Fig. 7, this does not necessarily imply that the energetic electron tail can be neglected in the low-temperature case.

The calculation of $H(\psi_d)$ in Eqn. 29 requires that dust grains be isolated; when grains strongly interact with each other, Havnes *et al.* [14] shows that the electron capture by dust grains is limited. Strongly-coupled grains require that the inter-particle spacing is smaller than the Debye length.[37] Because the ion Debye length is smaller than the electron Debye length, Debye shielding of the dust grain is largely determined by the ions. This Debye length will become large when the ions (as well as electrons) are depleted. This depletion is typical when plasma density is smaller than dust density, such as in Pluto's atmosphere[36] and the dustiest regions of protoplanetary disks.[34]

The analytical approach outlined in earlier sections is applied to three of the plasmas in Table II with similar neutral densities: noctilucent clouds, protoplanetary disks, and Pluto's aerosols. In Fig. 9, relations from Eqn. 29 are plotted in black for three different recombination times (1s, 0.1s, 0.01s) and for a Maxwellian distribution, and two different neutral gases (He and N_2). In red, the relation from Eqn. 32 is plotted for the dust densities and sizes in each of the three plasmas considered. Intersection points between each red line and the applicable black lines are highlighted in blue. Notably, the larger the high-energy tail of the distribution, the more rightward the $H(\psi_d)$ curve shifts. This can cause the dust charge and free electron depletion in equilibrium to be much larger than for otherwise-identical dust and plasma conditions when electrons are cold and Maxwellian.

From Fig. 9, both noctilucent clouds and protoplanetary disks have equilibrium values widely different depending on which electron distribution is used. The effect is less prominent for Pluto's atmosphere: as the density of aerosols in Pluto's atmosphere is much higher than the plasma density, electrons are completely depleted and H approaches 1 regardless of the electron distribution used. ψ_d is also small, as even when 100 percent of electrons are attached to grains, not every grain is charged: Monte Carlo simulation with the same properties used in Fig. 9 show an average grain charge of 0.0002.

Protoplanetary disks can have grain sizes and densities ranging over several orders of magnitude depending on their position in the disk and the stage of the disk's time evolution, as listed in Table II. The values plotted in Fig. 9 are roughly

TABLE II. Typical dusty plasma properties in a range of planetary and space environments. These are nominal parameters, and in general, all these plasmas have substantial ranges of parameters. Electron temperatures are based on average measured or predicted energies, and ignore non-Maxwellian effects.

	Neutral density (cm^{-3})	Plasma density (cm^{-3})	Grain density (cm^{-3})	Grain diameter (μm)	Neutral temperature (eV)	Electron temperature (eV)	Charge number (e)	Neutral gases	Reference
Comet tail	10^8-10^9	10^2-10^3	–	0.1-1	0.01	0.01	–	H_2O	9
Saturn's AB ring	10^3	40	10^{-2}	1	0.01	5	10^3	O, H_2O, O_2	31
Saturn's G ring	10^3	10	10^{-7}	1	0.01	1	10^3	O, H_2O, O_2	2
Molecular clouds	10^6	1	$< 10^{-3}$	0.1	0.0001	1	100	H_2, He	32,33
Protoplanetary disk	10^{14}	10^2	10^{-9}-10^6	0.01-1000	0.01	0.01	$1-10^4$	H, He	34,35
Noctilucent clouds	10^{14}	4000	0-1000	10^{-3}-10^{-1}	0.01	0.01	1	N_2, O_2	6
Pluto's aerosols	10^{13}	10^2-10^3	10^6	0.01-100	0.01	0.005-0.01	1-10^3	N_2	8,36

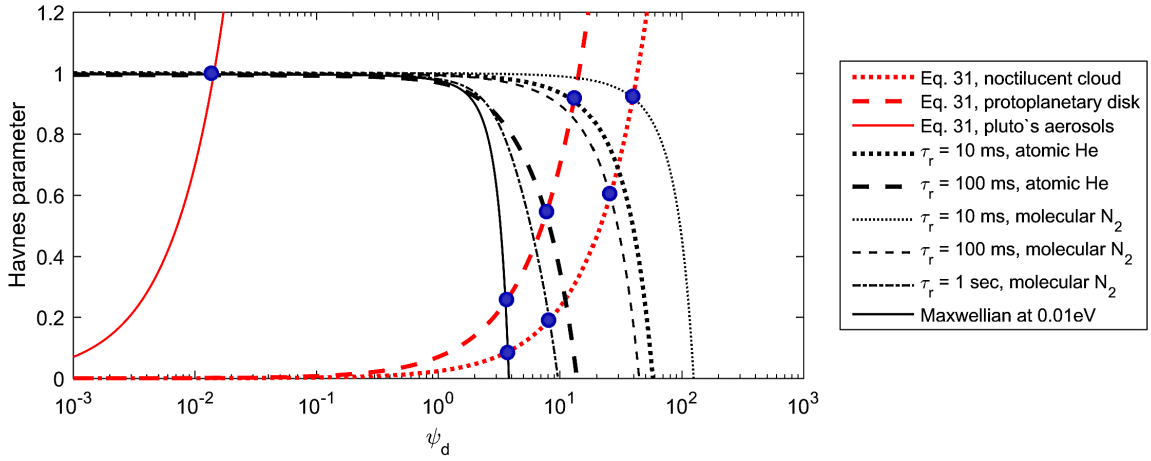

FIG. 9. Black downsloping lines are from Eq.29 for four cases using the electron moderation model and for a maxwellian electron distribution; red upsloping lines are from Eq.32 for typical noctilucent clouds ($r_d = 0.01\mu$m, $n_d = 1000$ cm^{-3}, $n_i = 4000$ cm^{-3}), protoplanetary disks ($r_d = 1\mu$m, $n_d = 1$ cm^{-3}, $n_i = 100$ cm^{-3}), and Pluto's aerosols ($r_d = 0.01\mu$m, $n_d = 10^6$ cm^{-3}, $n_i = 10^3$ cm^{-3}). All cases have neutral density of 10^{14} cm^{-3} and neutral temperature 0.01 K. Intersections of upsloping and downsloping lines shown as filled blue circles give equilibrium values of H and ψ_d for the specific configuration.

in the middle of their possible ranges: grains of radius 1μm and densities of 10^2 cm^{-3}. Based on the figure, the equilibrium values of H and ψ_d for these grains may vary widely depending on the average electron lifetime.

The typical lifetime of electrons under the protoplanetary disk conditions in Table II is now calculated. In the absence of dust, electron lifetime depends on the rate of electron-ion collisions: $\tau_{ei} = 1/\sigma_i n_i v_e$. Calculating cross section from Eqn. 16 for a singly-charged ion with radius of 1 angstrom, and considering an electron with energy of 0.01 eV, $\tau_{ei} \sim 1$ hr. Following the 1 hr line from Fig. 4, the probability of an electron having 0.1 eV is 10^{-5}, and continues to drop for higher energies. The product of this probability with electron density of 10^2 cm^{-3} (from Table II) is < 0.001 cm^{-3}. Therefore, it is unlikely that any hot electrons would be present in any given 1 cm^3 volume. In the presence of dust, however, electron lifetime can vastly decrease due to their collection by dust grains. For the dust size and density in Fig. 9 and an electron with an energy of 0.01eV, the electron-dust collision time is $\tau_{ed} = 1/\sigma_d n_d v_e \sim 5$ seconds for an uncharged dust grain, as calculated from Eqn. 26. This causes an increase in the proportion of hot electrons, and results in increases of both H and ψ_d.

The densities of neutrals, plasma, and dust all vary with time as protoplanetary disks evolve. As the star accretes mass, neutral density drops, decreasing the cooling rate of electrons and thus increasing their energy distribution's high-energy tail. As dust particles grow, the cross-section for electron capture changes as well, causing both higher grain charging and more depletion of both electrons and ions. As the grain charge in dust clouds has been shown to affect their coagulation rate,[4] and the density of plasma particles influences the mass accretion of the disk into its host star[35], these effects can have significant influence on observable dynamics of these disks.

While most of the aforementioned dusty plasmas are far from Earth, and so direct measurements of any such properties are few to non-existent, charging of dust and ice in the summer polar mesosphere has been directly detected. Under

the conditions in which noctilucent clouds and polar mesospheric summer echoes are observed, there are bite-outs in the electron density profile of up to an order of magnitude,[38] associated with the presence of charged ice-dust particles detected by Havnes *et al.*[5]. Charged particles of sizes of 10-20 nm in diameter were shown to exist in several atmospheric layers, carrying charge from absorbed electrons. Havnes *et al.*[5] assumes that these particles are singly-charged, and thus have number densities on the order of 10^3 per cubic centimeter. Larger grains, which appear during noctilucent cloud events, have lower densities and have been detected to sometimes carry positive charges due to photoemission.[5,6]

From Fig. 9, H could be anywhere between 0.1 and 0.9, and ψ_d from 4 to 40, depending on the recombination time. In these layers of the mesosphere, electron production is mainly due to photoionization of NO molecules. The α coefficient for recombination with NO+ ions is between $10^{-7} - 10^{-5}$ cm ^{3} s^{-1},[6] depending on elevation and solar conditions. This results in average recombination times ($1/\alpha n_i$) of tens of seconds to several minutes, meaning that equilibrium values will be closer to the intersection with the Maxwellian curve. However, this means that each grain has less than one charge. Since the analytical method does not take into account charge discretization, it may give unreliable results in this range. The presence of dust also causes electron lifetime to get shorter, as it preferentially absorbs high-energy (younger) electrons. To accommodate these effects, the Monte Carlo method is used.

Simulation results show that this plasma is in the $t_R/t_{en} >> x_c$ regime, such that the hot tail is small, as predicted by the analytical method. For the 10nm grains at 1000 cm^{-3}, the simulation gives $\psi_d = 12.6$, which corresponds to an average charge of $Z_d = 0.877$; specifically, 12% are uncharged, 87.9% are singly-charged, and 0.1% are doubly-charged. The Havnes parameter is calculated to be $H = 0.42$.

Using the aerosol charging model developed by Parthasarathy[39] to calculate the dust charge distribution and an iterative process to find equilibrium values, Rapp and Lübken[6] calculated electron and ion densities in the presence of mesospheric dust. For 10nm grains at 1000 cm^{-3}, the Havnes parameter is calculated from their electron and ion densities to be $H = 0.33$, roughly 25% lower than that predicted by our model. From Eqn. 32, $\psi_d = 14.4$, so their method predicts an average Z_d of exactly 1. This is lower than the average charge calculated by our simulation, which indicates that there is not only more electron depletion, but also more ion depletion in our model than in Rapp and Lubken's calculation. As their dust distribution was calculated from Natanson[40] assuming a thermal distribution, it neglects the higher probability of electron-dust collision for electrons that are hotter than the cold bulk. The higher electron capture rate in turn enhances ion absorption, and is capable of causing the larger bite-outs in electron and ion density profiles, such as those observed in these mesospheric layers.

VII. SUMMARY

In a dusty plasma, the charge developed on isolated dust grains in equilibrium is dependent on the energy distributions of the charged particles colliding with the dust. While most studies of dusty plasmas implicitly assume Maxwellian distributions, this is not always the case, a consequence that has important implications for the properties of the dust.

A model is presented for a dusty plasma based on neutron moderation used in fission reactors. In this model, free electrons are created and accelerated by a constant ionization source, cool down through collisions with the colder neutral population, and then recombine with an ion or a dust grain. It is found that, even for long recombination times in which electrons undergo many collisions with neutrals, the electron distribution contains a high-energy tail of greater magnitude than that of a Maxwellian distribution. The model only accounts for isolated dust grains, that is, when dust interparticle spacing is larger than the ion Debye length.

The dust accumulates charge through collisions with ions and electrons, eventually reaching a steady-state average charge when electron-dust and ion-dust collision rates equate. It is shown that this equilibrium charge is greatly affected by the highest-energy electrons, as these can approach charged dust grains that would repel colder electrons. These higher-charged grains can then attract more ions to their surfaces as well. The increased dust charge comes at the expense of free electrons in the plasma, causing higher depletion in the electron density where dust is present. The high-energy tail predicted by the electron moderation model therefore significantly changes both the expected dust charge and the charge distribution throughout the dusty plasma. As many naturally occurring dusty plasmas, including the Earth's mesosphere, protoplanetary disks, extraterrestrial atmospheres, and molecular clouds, are ionized by radiation that produces energetic electrons, estimates of charge on dust grains in terrestrial and space environments may be significantly underestimated.

VIII. ACKNOWLEDGEMENTS

This material is based upon work supported by a NSF/DOE Partnership in Plasma Science and Engineering via DOE Award DE-SC0020079.

Appendix A: Calculation of the electron distribution for non-negligible spread of electron lifetime

Details for calculating the probability that an electron remains free are as follows. As given Eq. A1, the chance that an electron has not recombined by a time $t + dt$ is given by $p(t + dt)$, which is the product of $p(t)$ and the probability of remaining free during dt:

$$p(t+dt) = p(t)\left(1 - n_i \sigma_R(w)\sqrt{\frac{2w}{m_e}}\right). \qquad \text{(A1)}$$

Expanding this,

$$p(t+dt) = p(t) + \frac{dp}{dt}dt = p(t)\left(1 - n_i\sigma_R(w)\sqrt{\frac{2w}{m_e}}dt\right) \quad \text{(A2)}$$

This simplifies to equation 10 in the text. Multiplying equation 10 by the inverse of equation 4, the differential equation for p can be written in terms of energy rather than time:

$$\frac{dp}{dw} = \frac{dp}{dt}\frac{dt}{dw} = \frac{n_i\sigma_R(w)w^{1/2}p(t)}{4\frac{m_e}{M}\sigma_n n_n(w^{3/2} - kT_n w^{1/2})} \quad \text{(A3)}$$

Now, the form of the recombination cross-section $\sigma_R(w)$ is assumed to be a power law of the form γ/w^{μ}. For recombination with a dust grain, $\mu = 1$, as shown by Eq. 16. Walls and Dunn [29] show that for the NO^+ recombination in the Earth's mesosphere, $\mu = 3/2$ over the relevant energy range. For the remainder of the equation, it will be assumed $\mu = 1$ for simplicity. Substituting this into eq. A3,

$$\frac{dp}{dw} = \frac{cw^{-1/2}p}{w^{3/2} - kT_n w^{1/2}} \quad \text{(A4)}$$

where,

$$c = \frac{1}{4}\frac{\gamma}{\sigma_n}\frac{n_i}{n_n}\frac{M}{m_e}. \quad \text{(A5)}$$

The differential equation is subject to the boundary condition $p(w = w(0)) = 1$, as no electrons recombine at their moment of ionization. The differential equation can then be solved as follows:

$$\begin{aligned} \frac{dp}{p} &= \\ d(\log p) &= \int \frac{cw^{-1/2}}{w^{3/2} - kT_n w^{1/2}}dw \\ &= c\int \frac{1}{w}\frac{1}{w - kT_n}dw \\ &= -c\int \frac{1}{kT_n}\left(\frac{1}{w} - \frac{1}{w - kT_n}\right)dw \\ &= -c\int \frac{1}{kT_n}\left(d(\log w) - d(\log(w - kT_n))\right)dw \end{aligned} \quad \text{(A6)}$$

Solving this results in:

$$p(w) = \kappa\left(\frac{w}{w - kT_n}\right)^{-c/kT_n} \quad \text{(A7)}$$

where κ is the constant of integration. Applying the boundary condition $p(w(0)) = 1$ results in equation 11 in the text.

Eq. 11 is plotted in Fig. 10 for varying values of c/kT_n. When c/kT_n decreases below 1, the drop from $p(w) = 1$ to $p(w) = 0$ happens more and more rapidly, and the spread in lifetime becomes more and more negligible. This justifies approximating $p(w)$ as a step function centered at $w(\tau_R)$ when c is small; as discussed in the text, c is typically very small for these dusty plasmas. This simplifies the normalization, as shown in Eq. 13.

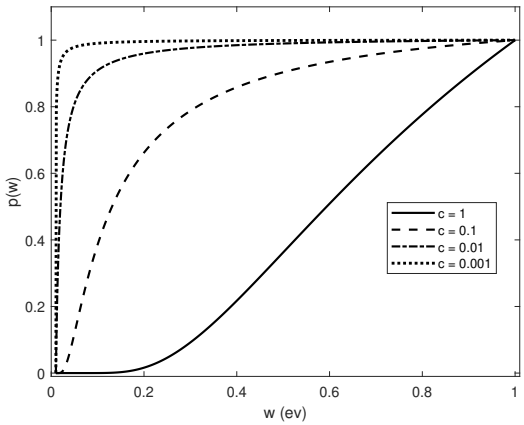

FIG. 10. Equation 11 plotted for $w(0) = 1$ eV and $kT_n = 0.01$ eV, for several values of c. Both the average recombination time and the spread in lifetimes decrease with c.

When the lifetime is very short, c starts to grow, and thus electrons have a larger spread of lifetimes. In this case, the normalization equation could be written as:

$$1 = A\int_{kT_n}^{w(0)} \frac{dw}{|dw/dt|}\left(\frac{w(0) - kT_n}{w(0)}\frac{w}{w - kT_n}\right)^{-c/kT_n}, \quad \text{(A8)}$$

and the integral could be solved numerically to obtain the correct normalization factor A.

[1] L. R. Danielsson and G. H. Kasai, "Laboratory simulation of plasma phenomena in comets," Journal of Geophysical Research (1896-1977) **73**, 259–266 (1968).

[2] C. J. Mitchell, M. Horányi, O. Havnes, and C. C. Porco, "Saturn's spokes: Lost and found," Science **311**, 1587–1589 (2006).

[3] P. M. Bellan, "Why Interstellar Ice Dust Grains Should Be Elongated," The Astrophysical Journal **905**, 96 (2020), publisher: American Astronomical Society.

[4] A. V. Ivlev, M. Padovani, D. Galli, and P. Caselli, "Interstellar dust charging in dense molecular clouds: cosmic ray effects," The Astrophysical Journal **812**, 135 (2015).

[5] O. Havnes, J. Trøim, T. Blix, W. Mortensen, L. I. Næsheim, E. Thrane, and T. Tønnesen, "First detection of charged dust particles in the earth's mesosphere," Journal of Geophysical Research: Space Physics **101**, 10839–10847 (1996).

[6] M. Rapp and F.-J. Lübken, "Modelling of particle charging in the polar summer mesosphere: Part 1general results," Journal of Atmospheric and Solar-Terrestrial Physics **63**, 759–770 (2001).

[7] C. Szopa, G. Cernogora, L. Boufendi, J. J. Correia, and P. Coll, "Pampre: A dusty plasma experiment for titan's tholins production and study," Planetary and Space Science **54**, 394–404 (2006).

[8] L. Jovanovi, T. Gautier, V. Vuitton, C. Wolters, J. Bourgalais, A. Buch, F.-R. Orthous-Daunay, L. Vettier, L. Flandinet, and N. Carrasco, "Chemical composition of pluto aerosol analogues," Icarus **346**, 113774 (2020).

[9] D. Mendis and M. Horányi, "Dusty plasma effects in comets: Expectations for rosetta," Reviews of Geophysics **51**, 53–75 (2013).

[10] K.-B. Chai and P. M. Bellan, "Study on morphology and growth of waterice grains spontaneously generated in a laboratory plasma," Journal of Atmospheric and Solar-Terrestrial Physics **127**, 83–91 (2015), layered Phenomena in the Mesopause Region.

[11] O. Vaste, "Noctilucent clouds," Journal of Atmospheric and Terrestrial Physics **55**, 133–143 (1993).

[12]O. Havnes, G. E. Morfill, and C. K. Goertz, "Plasma potential and grain charges in a dust cloud embedded in a plasma," Journal of Geophysical Research: Space Physics **89**, 10999–11003 (1984).
[13]S. Kopnin, I. Kosarev, S. Popel, and M. Yu, "Localized structures of nano-size charged dust grains in earth's middle atmosphere," Planetary and Space Science **52**, 1187–1194 (2004).
[14]O. Havnes, C. K. Goertz, G. E. Morfill, E. Grün, and W. Ip, "Dust charges, cloud potential, and instabilities in a dust cloud embedded in a plasma," Journal of Geophysical Research: Space Physics **92**, 2281–2287 (1987).
[15]P. M. Bellan, *Fundamentals of Plasma Physics.* (Cambridge University Press, 2006).
[16]F. F. Chen, "Langmuir probes in rf plasma: surprising validity of oml theory," Plasma Sources Science and Technology **18**, 035012 (2009).
[17]P. K. Shukla and A. A. Mamun, *Introduction to dusty plasma physics* (Inst. of Physics Publ., 2002).
[18]V. M. Vasyliunas, "A survey of low-energy electrons in the evening sector of the magnetosphere with ogo 1 and ogo 3," Journal of Geophysical Research (1896-1977) **73**, 2839–2884 (1968).
[19]P. C. Stangeby, "A problem in the interpretation of tokamak Langmuir probes when a fast electron component is present," Plasma Physics and Controlled Fusion **37**, 1031–1037 (1995), publisher: IOP Publishing.
[20]K.-B. Chai and P. M. Bellan, "Spontaneous formation of nonspherical water ice grains in a plasma environment," Geophysical Research Letters **40**, 6258–6263 (2013).
[21]United States Department of Energy, *Department of Energy Fundamentals Handbook: Nuclear physics and reactor theory*, Vol. 2 (1993).
[22]L. Huxley, "Formulae for the mean losses of energy in collisions of slow electrons moving in diatomic gases," Australian Journal of Physics **9**, 44–53 (1956).
[23]D. Smith and A. Dean, "Electron temperature relaxation rates in flowing afterglow plasmas containing molecular nitrogen and oxygen," Journal of Physics B: Atomic and Molecular Physics **8**, 997 (1975).
[24]G. C. Reid, "Production and loss of electrons in the quiet daytime d region of the ionosphere," Journal of Geophysical Research (1896-1977) **75**, 2551–2562 (1970), https://agupubs.onlinelibrary.wiley.com/doi/pdf/10.1029/JA075i013p02551.
[25]H. Kimura, "On the photoelectric quantum yield of small dust particles," Monthly Notices of the Royal Astronomical Society **459**, 2751–2761 (2016).
[26]M. I. Al-Joboury and D. W. Turner, "985. molecular photoelectron spectroscopy. part i. the hydrogen and nitrogen molecules," J. Chem. Soc. , 5141–5147 (1963).
[27]R. Johnson, J. Luhmann, R. Tokar, M. Bouhram, J. Berthelier, E. Sittler, J. Cooper, T. Hill, H. Smith, M. Michael, M. Liu, F. Crary, and D. Young, "Production, ionization and redistribution of o2 in saturn's ring atmosphere," Icarus **180**, 393–402 (2006).
[28]O. Engvold, J. C. Vial, and A. Skumanich, *The Sun as a guide to Stellar Physics* (Elsevier, 2019).
[29]F. Walls and G. Dunn, "Measurement of total cross sections for electron recombination with no+ and o2+ using ion storage techniques," Journal of Geophysical Research **79**, 1911–1915 (1974).
[30]J. Allen, R. Boyd, and P. Reynolds, "The collection of positive ions by a probe immersed in a plasma," Proceedings of the Physical Society. Section B **70**, 297 (1957).
[31]V. Yaroshenko, F. Verheest, and G. Morfill, "Dust-acoustic waves in collisional dusty plasmas of planetary rings," Astronomy & Astrophysics **461**, 385–391 (2007).
[32]F. H. Shu, F. C. Adams, and S. Lizano, "Star formation in molecular clouds: observation and theory," Annual review of astronomy and astrophysics **25**, 23–81 (1987).
[33]V. Zubko, E. Dwek, and R. G. Arendt, "Interstellar dust models consistent with extinction, emission, and abundance constraints," The Astrophysical Journal Supplement Series **152**, 211 (2004).
[34]P. J. Armitage, *Astrophysics of Planet Formation*, 2nd ed. (Cambridge University Press, 2020).
[35]Y. Zhang and P. M. Bellan, "Neutral-charged-particle collisions as the mechanism for accretion disk angular momentum transport," The Astrophysical Journal **930**, 167 (2022).
[36]X. Zhu, D. F. Strobel, and J. T. Erwin, "The density and thermal structure of plutos atmosphere and associated escape processes and rates," Icarus **228**, 301–314 (2014).
[37]P. Bellan, "A model for the condensation of a dusty plasma," Physics of Plasmas **11**, 3368–3379 (2004).
[38]E. J. Jensen and G. E. Thomas, "Charging of mesospheric particles: Implications for electron density and particle coagulation," Journal of Geophysical Research: Atmospheres **96**, 18603–18615 (1991).
[39]R. Parthasarathy, "Mesopause dust as a sink for ionization," Journal of Geophysical Research **81**, 2392–2396 (1976).
[40]G. Natanson, "On the theory of the charging of amicroscopic aerosol particles as a result of capture of gas ions," Sov. Phys. Tech. Phys. **30**, 573–588 (1960).